

A Wave Amplitude Transition in a Quasi-Linear Model with Radiative Forcing and Surface Drag

ORLI LACHMY AND NILI HARNIK

Tel-Aviv University, Tel Aviv, Israel

(Manuscript received 26 March 2009, in final form 27 May 2009)

ABSTRACT

A quasi-linear two-layer quasigeostrophic β -plane model of the interaction between a baroclinic jet and a single zonal wavenumber perturbation is used to study the mechanics leading to a wave amplitude bifurcation—in particular, the role of the critical surfaces in the upper-tropospheric jet flanks. The jet is forced by Newtonian heating toward a radiative equilibrium state, and Ekman damping is applied at the surface. When the typical horizontal scale is approximately the Rossby radius of deformation, the waves equilibrate at a finite amplitude that is comparable to the mean flow. This state is obtained as a result of a wave-induced temporary destabilization of the mean flow, during which the waves grow to their finite-equilibrium amplitude. When the typical horizontal scale is wider, the model also supports a state in which the waves equilibrate at negligible amplitudes. The transition from small to finite-amplitude waves, which occurs at weak instabilities, is abrupt as the parameters of the system are gradually varied, and in a certain range of parameter values both equilibrated states are supported.

The simple two-layer quasi-linear setting of the model allows a detailed examination of the temporary destabilization process inherent in the large-amplitude equilibration. As the waves grow they reduce the baroclinic growth by reducing the vertical shear of the mean flow, and reduce the barotropic decay by reducing the mean potential vorticity gradient at the inner sides of the upper-layer critical levels. Temporary destabilization occurs when the reduction in barotropic decay is larger than the reduction in baroclinic growth, leading to a larger total growth rate. Ekman friction and radiative damping are found to play a major role in sustaining the vertical shear of the mean flow and enabling the baroclinic growth to continue. By controlling the mean flow potential vorticity gradient near the critical level, the model evolution can be changed from one type of equilibration to the other.

1. Introduction

Abrupt changes in the equilibrated wave–mean flow state are found in a range of atmospheric models that simulate the midlatitude tropospheric dynamics (e.g., Thorncroft et al. 1993; Hartmann and Zuercher 1998; Son and Lee 2005; Robinson 2006; Swanson 2008). By “abrupt” we mean a sharp transition when an external parameter is varied slowly.

In many of these studies, the sharp transition arises because of a change in the barotropic part of the dynamics, in particular that part involving the upper-tropospheric critical level (CL; where the wave’s phase speed equals the mean flow wind). At the most basic level, the existence of a CL shifts the dynamics from

having eddy life cycles of baroclinic dominance during both the growth and decay stages to life cycles in which the decay is barotropic (Feldstein and Held 1989). This introduces a strong sensitivity of the dynamics to the CL region, which can give rise to regime transitions under the right circumstances. This strong sensitivity to the reflection or absorption properties of the CL is found in a range of studies (e.g., Feldstein and Held 1989; Lee and Held 1991; Barnes and Young 1992; Thorncroft et al. 1993; Hartmann and Zuercher 1998; Esler and Haynes 1999; Robinson 2006), but the dynamical mechanism by which the CL affects the equilibrated state is not fully understood.

There are detailed idealized studies of the dynamics of a wave impinging on a CL (Warn and Warn 1978; Killworth and McIntyre 1985) that suggest that in the nonlinear limit a CL can undergo cycles of absorption, reflection, and overreflection, settling at the end on a fully reflective state. However, these studies focus on the

Corresponding author address: Orli Lachmy, Department of Geophysics, Tel-Aviv University, Tel Aviv 69978, Israel.
E-mail: orlipast@post.tau.ac.il

CL dynamics alone. To understand how the CL will affect the wave–mean flow equilibration, an understanding of the CL dynamics needs to be combined with other factors of the dynamics of the full system and their interplay.

The equilibrated state also depends on the radiative forcing and Ekman damping imposed. In the most simplistic view of baroclinic adjustment, waves try to neutralize the flow while forcing brings it closer to radiative equilibrium, allowing waves to keep being present (e.g., Barnes and Young 1992). However, the role of Ekman damping in maintaining baroclinicity is more complex—Robinson (2000, 2006) suggests that Ekman damping, by reducing the surface winds created by eddy momentum fluxes and increasing the vertical shear, allows the waves to reach a self-maintaining jet. A similar role for Ekman damping was found by Lee and Held (1991), in which this maintenance of vertical shear allowed subcritical instability to exist.

A common approach in studying wave–mean flow systems is to distinguish between quasi-linear wave–mean flow interactions and nonlinear wave–wave interactions. In this study, we examine the quasi-linear answer to the following question: How mechanistically, if at all, does the CL affect the wave–mean flow equilibration? How does the dynamical interplay among baroclinic growth, the CL region, Ekman damping, and thermal forcing determine the equilibrated wave–mean flow state and the existence of sharp transitions between dynamical regimes? We view this quasi-linear answer as a basis for understanding similar transition processes in the full system.

By ignoring the messy nonlinear part of the dynamics, we gain numerical and conceptual simplicity, which allows a more thorough and systematic examination of the dynamics, as well as a mechanistic understanding of specific dynamical components and how they mutually interact. While nonlinear interactions are necessary to realistically simulate the time evolution, as well as the explicit dependence of the equilibrated state on model parameters, we can still get a relevant physical understanding of the behavior of the system by ignoring their effect. There are studies that support the ability of quasi-linear dynamics to capture many essential features of the circulation, especially at weak supercriticalities (Haynes and McIntyre 1987; Feldstein and Held 1989; Lee and Held 1991; O’Gorman and Schneider 2007). Although theories of geostrophic turbulence and eddy diffusivity are found to give good predictions for the fully nonlinear system at high supercriticalities, their predictions at low supercriticalities are not as accurate, presumably because they assume the existence of an inverse energy cascade and neglect the contribution of momentum fluxes to potential vorticity (PV) mixing (e.g., Held and Larichev 1996; Zurita-Gotor 2007). Because the atmosphere is generally close to neutrality (Stone 1978) and includes

only weak wave–wave interactions (Schneider and Walker 2006), a study of the processes that control the quasi-linear model may be of relevance.

We use a two-layer quasigeostrophic β -plane model, radiatively forced toward an upper-layer jet with zero surface wind, on which a single zonal wavenumber evolves in the presence of Ekman damping. We perform a series of initial value runs, integrated to statistical equilibrium, for different values of the model parameters. This is the most obvious choice for such a study because it is the simplest model that captures baroclinic instability with barotropic processes and it is known to exhibit different wave–mean flow regimes (e.g., Feldstein and Held 1989; Lee and Held 1991). Lee and Held (1991) also showed that this model exhibits subcritical instability and hysteresis and they found strong evidence, if not outright proof, of a major role for the CL region through PV mixing and meridional wave reflection. Here we will concentrate more on the unstable model regime, which exhibits a similar wave amplitude transition, and examine explicitly the role of the CL. We will make use of the PV kernel approach of Heifetz and Methven (2005), which views the emerging waves in terms of an interaction of the PV perturbation in different parts of the wave field.

The model assumptions and numerical methods are described in section 2. The destabilization of the mean flow by the wave is studied in section 3, focusing on a certain example. The abrupt transition of the wave amplitude, as a function of the model parameters or initial conditions, is studied in section 4. The maintenance of the statistically steady state with finite wave amplitude is investigated in section 5. Section 6 gives a summary and concluding remarks.

2. Model description

We use a standard two-layer β -plane quasigeostrophic model (e.g., Phillips 1951). The model solves the following mean flow equations (nondimensionalized as in Table A1 in the appendix):

$$\frac{\partial \bar{U}_M}{\partial t} = -\frac{\partial}{\partial y}(\overline{u'v'})_M - \frac{Ek}{2}(\bar{U}_M - 2\bar{U}_T), \quad (1)$$

$$\begin{aligned} \frac{\partial \bar{U}_T}{\partial t} = \bar{v}_{aT} - \frac{\partial}{\partial y}(\overline{u'v'})_T \\ + \frac{Ek}{2}(\bar{U}_M - 2\bar{U}_T), \quad \text{and} \end{aligned} \quad (2)$$

$$\begin{aligned} \left(\frac{\partial^2}{\partial y^2} - 2\lambda^2\right)\bar{v}_{aT} = -2\lambda^2 \left[\frac{\partial}{\partial y}(\overline{u'v'})_T + \frac{\partial^2}{\partial y^2}(\overline{v'_M \psi'_T}) \right] \\ + \lambda^2 Ek(\bar{U}_M - 2\bar{U}_T) \\ + 2\lambda^2 \alpha(\bar{U}_T - U_{\text{Trad}}). \end{aligned} \quad (3)$$

The model also solves the wave equations:

$$\frac{\partial q'_M}{\partial t} = -ik \left[\bar{U}_M q'_M + \bar{U}_T q'_T + \left(\frac{\partial \bar{q}}{\partial y} \right)_M \psi'_M + \left(\frac{\partial \bar{q}}{\partial y} \right)_T \psi'_T \right] - \frac{Ek}{2} (\zeta'_M - 2\zeta'_T), \quad \text{and} \quad (4)$$

$$\frac{\partial q'_T}{\partial t} = -ik \left[\bar{U}_M q'_T + \bar{U}_T q'_M + \left(\frac{\partial \bar{q}}{\partial y} \right)_M \psi'_T + \left(\frac{\partial \bar{q}}{\partial y} \right)_T \psi'_M \right] + \frac{Ek}{2} (\zeta'_M - 2\zeta'_T) + 2\lambda^2 \alpha \psi'_T, \quad (5)$$

where ψ' , q' , ζ' , u' , and v' are the perturbation streamfunction, PV, vorticity, and zonal and meridional geostrophic winds, respectively; \bar{U} and \bar{q} are mean flow zonal wind and PV, respectively; \bar{v}_a is the mean ageostrophic meridional wind; y is latitude; and k is the perturbation zonal wavenumber. In all model runs we took the most unstable normal mode of the initial mean flow as the initial condition for the perturbation, so that k is the wavenumber that gives maximum instability. We have written the variables in terms of their barotropic and baroclinic components: $p_M \equiv \frac{1}{2}(p_1 + p_2)$, $p_T \equiv \frac{1}{2}(p_1 - p_2)$, where p_1 and p_2 are any upper- and lower-layer variables, respectively. The notation is standard and appears in the appendix.

Equation (3), for the mean meridional circulation, was obtained using the mean temperature equation, together with the thermal wind relation. Equations (1)–(5) depend on four nondimensional parameters (explicitly described in Table A2 in the appendix)—Newtonian and Ekman damping coefficients (α , Ek); nondimensional β ; a horizontal length scale parameter (λ), which represents the importance of vortex stretching, relative to vorticity, in determining the PV; and the radiative equilibrium profile U_{Trad} . In all experiments, unless specified otherwise, we chose U_{Trad} to be equal to

$$U_{\text{Trad}} = \frac{1}{3} \exp \left[- \left(\frac{4y}{y_{\text{max}}} \right)^2 \right], \quad (6)$$

where $\pm y_{\text{max}}$ are the boundaries of the domain, taken to be far enough to have no effect on the dynamics. Unless specified otherwise, $y_{\text{max}} = 5$, so that the jet width is approximately 1. For the Ekman friction we assume that the wind varies linearly with height and that the friction depends on the wind at the surface. The numerical setup is described in more detail in the appendix.

3. The destabilization process

A series of experiments was conducted with different values of the parameters λ , Ek , α , and β . The results can be divided into two distinct groups—experiments in

which the final wave amplitude was comparable to the mean flow and experiments in which the wave equilibrated at a small enough amplitude to not greatly affect the mean flow. The parameter ranges in which the two regimes appeared and the transitions between them are discussed in section 4. In this section we wish to reveal the processes leading to the large-amplitude state. Most cases explored in this work are in the range of weak linear instability of the initial state (growth rate is smaller than 0.1). A few cases with larger instability were investigated for comparison and will be discussed later. In all cases that started with weak instability and ended with a large amplitude, the instantaneous growth rate of the wave was found to increase with time for a limited period, indicating a destabilization of the mean flow. This result may be surprising because the wave grows at the expense of the energy of the mean flow and therefore we would expect it to stabilize the mean flow.

To understand the destabilization process, we focus on a case study with specific parameters: $\lambda = 1.5$, $Ek = 0.1$, $\alpha = 0.05$, and $\beta = 0.5$. These parameter values are close to the atmospheric ones but correspond to a slightly larger wind speed, larger meridional scale, and shorter radiative damping time scale. Inserting atmospheric values gives a stable mean flow. The wavenumber in this case is $k = 1.6$.

Figure 1 shows the domain-averaged eddy kinetic energy [$\frac{1}{2}(u'^2 + v'^2)$] and instantaneous growth rate (half the logarithmic time derivative of the eddy kinetic energy) as a function of time, along with the linear growth rate, which is the growth rate of the most unstable normal mode. The instantaneous growth rate increases between $t = 6$ and $t = 17$, reaching a value almost 4 times the initial value at $t = 17$, after which it decreases slowly toward zero while oscillating, and eventually a steady state is reached with finite wave amplitude. The instantaneous growth follows the linear one with some delay, which suggests that the temporal increase in the instantaneous growth rate represents a “linear” destabilization and not, for example, nonmodal growth.¹

Figure 2 shows the mean flow zonal wind and PV gradient at both layers at $t = 0$ (the linear growth stage) and $t = 17$ (time of maximal growth rate). The vertical lines mark the location of the CLs.² The zonal wind is

¹ The absence of a clear linear growth stage in Fig. 1 is due to the fact that at these small growth rates, even the initial changes the wave induces on the mean flow are enough to affect the linear growth rate in a significant way. When the model is initiated with a perturbation 10 times smaller, a linear growth stage is seen.

² The instantaneous phase speed was calculated to determine the location of the CL. The phase speed changed during the model run in the range of 0.3 ± 0.05 , which did not change the location of the CL considerably, taking into account also the changes in the mean flow.

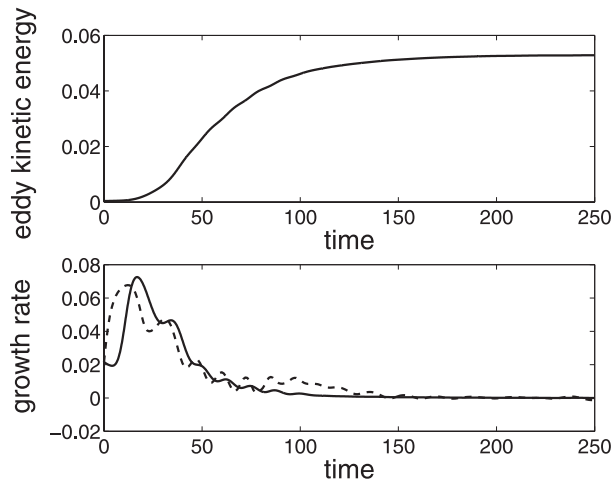


FIG. 1. Eddy kinetic energy and growth rate as a function of time for the model parameters $\lambda = 1.5$, $\beta = 0.5$, $\text{Ek} = 0.1$, and $\alpha = 0.05$. The solid line in the lower figure marks the instantaneous growth rate and the dashed line marks the linear growth rate of the most unstable normal mode.

only slightly changed—a closer inspection shows some decrease in the zonal wind on the inner sides of the CLs, which are located at $y \approx \pm 1.4$, and some increase at the center at both layers, indicating inward momentum flux. The PV gradient exhibits a substantial decrease at the upper layer on the inner sides of the CLs and an increase on the outer side. Some mild changes in the PV gradient are seen in the lower layer.

Figure 3 shows the wave PV (q') and streamfunction (ψ') as a function of x and y for both layers at $t = 0$. The thick solid lines mark the location of the CLs. Figure 4 shows the same variables at $t = 17$. The thick dashed lines mark the local minima of the mean PV gradient. The along shear meridional tilt of ψ' in the upper layer decreases from $t = 0$ to $t = 17$, indicating a weakening of the barotropic decay. At the same time the vertical phase tilt of ψ' slightly decreased, slightly weakening the baroclinic growth. The decrease in barotropic decay can provide an explanation for the increase in growth rate.

We view ψ' as being induced by q' , following the PV kernel approach of Heifetz and Methven (2005). Looking at q' , we see that its amplitude at the jet flanks decreased, relative to the center in the upper layer, at $t = 17$, relative to $t = 0$ (this is apparent by the disappearance of the local maximum of q' near the CL), whereas its meridional phase tilt decreased significantly in the region close to the CL. To check whether the change in ψ' originates in a change in the amplitude or phase structure of q' , we calculated the ψ' that would have been induced by a PV perturbation having the phase structure of q' at $t = 0$ and the amplitude structure of q' at $t = 17$, and vice versa. We found that in this case most

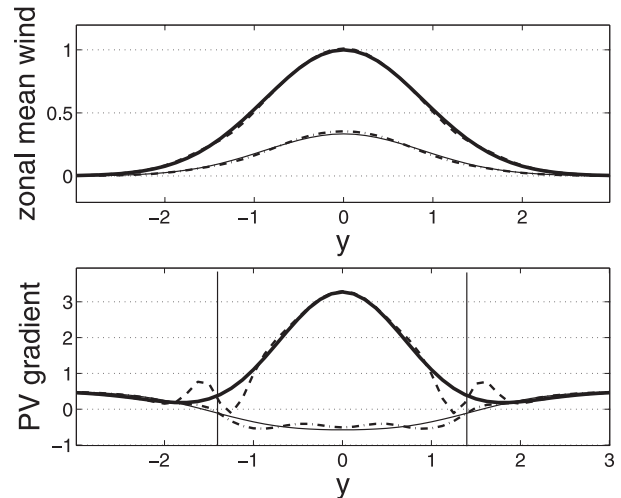


FIG. 2. Zonal mean wind and PV gradient for the upper layer at $t = 0$ (thick solid) and $t = 17$ (dashed) and for the lower layer at $t = 0$ (thin solid) and $t = 17$ (dashed-dotted) for the case $\lambda = 1.5$, $\beta = 0.5$, $\text{Ek} = 0.1$, and $\alpha = 0.05$. The vertical lines mark the location of the CLs.

of the change in the phase tilt of ψ' results from a change in the phase structure of q' , although in other model runs in which destabilization occurred we found more significance to the change in the amplitude structure of q' . We conclude that both the reduction in the phase tilt of q' near the CLs and the amplitude decrease at the jet flanks contribute to the reduction in barotropic decay.

Because the wave equations are linear and depend only on the mean flow, any change in the wave structure is caused by a change in the mean flow. We have seen that the mean PV gradient decreases on the inner sides of the CLs in the upper layer. To see how this can explain the change in the wave structure, we use the formulation of Heifetz and Methven (2005): We express q' in terms of amplitude and phase: $q' = Qe^{i\epsilon}e^{ikx}$, where Q and ϵ are real and depend on space and time, and express ψ' in terms of its contributions from q' at different locations using a Green function G : $\psi'_i(y, x) = \sum_{\hat{y}, j} G(y - \hat{y}, i, j) q'(\hat{y}, x, j)$, where i, j are layer indices (one upper, two lower), with j indicating the contributing PV layer and i the layer we are looking at. We then divide Eqs. (4) and (5) by q' and look at the real and imaginary parts, omitting the nonconservative terms of radiative damping and Ekman friction, to get the instantaneous phase speed $\hat{\epsilon}/k$ and growth rate \hat{Q}/Q due to PV advection:

$$\left(\frac{\hat{\epsilon}}{k}\right)_i(y) = \bar{U} + [\bar{q}_y(y)]_i \sum_{\hat{y}, j} G(y - \hat{y}, i, j) \frac{Q(\hat{y}, j)}{Q(y, i)} \times \cos[\epsilon(\hat{y}, j) - \epsilon(y, i)], \quad \text{and} \quad (7)$$

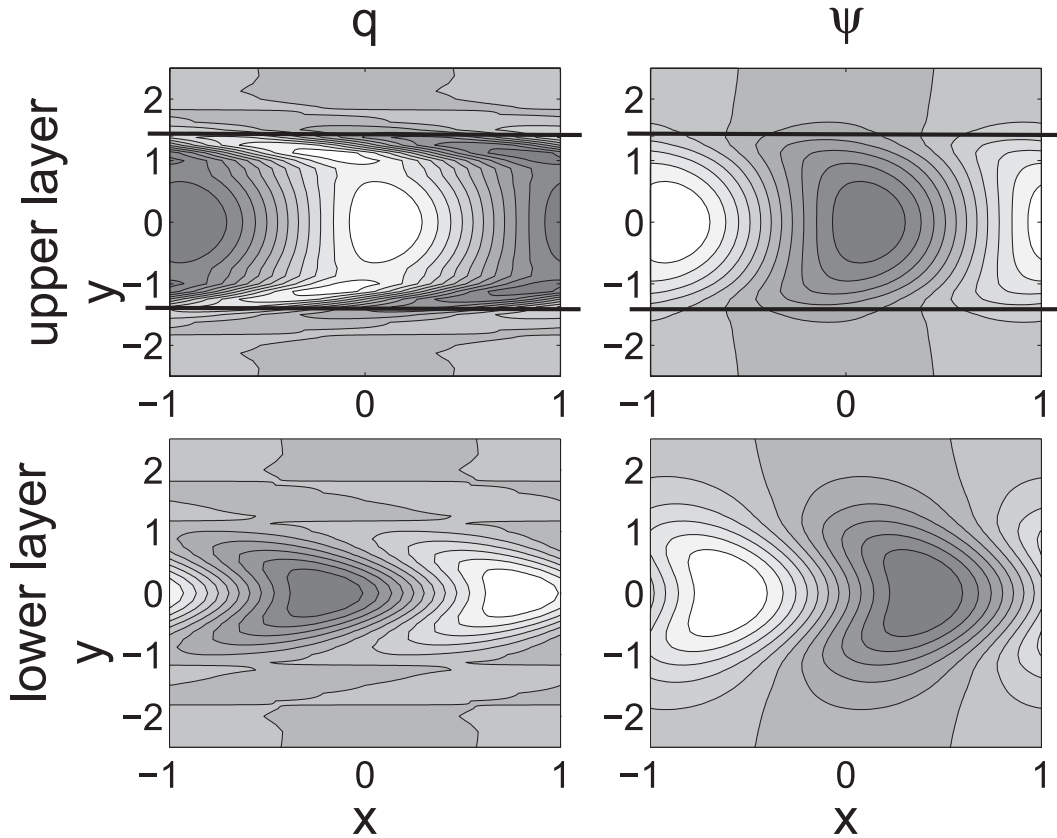


FIG. 3. Wave PV (q') and streamfunction (ψ') for the case $\lambda = 1.5, \beta = 0.5, Ek = 0.1,$ and $\alpha = 0.05$ at $t = 0$. The thick solid lines mark the location of the CLs.

$$\left(\frac{\dot{Q}}{Q}\right)_i(y) = k[\bar{q}_y(y)]_i \sum_{\hat{y}, j} G(y - \hat{y}, i, j) \frac{Q(\hat{y}, j)}{Q(y, i)} \times \sin[\varepsilon(\hat{y}, j) - \varepsilon(y, i)]. \tag{8}$$

The change in the wave PV phase structure is explained by looking at Eq. (7): at the CL the second term on the RHS should vanish. In a discrete model the CL is not resolved, but at a point close to the CL this term should be close to zero. If \bar{q}_y there is large, the sum multiplying it should be nearly zero. The sum is over all points in space, including the point we are looking at, for which $\cos[\varepsilon(\hat{y}, j) - \varepsilon(y, i)]$ equals 1, and the Green function is maximal. In order for the sum to be small other points in space should cancel the contribution of the point itself. This can be achieved only with a strong phase tilt, which would give negative values of $\cos[\varepsilon(\hat{y}, j) - \varepsilon(y, i)]$ close to the point we are looking at (the Green function decays exponentially with $|y - \hat{y}|$). As \bar{q}_y decreases near the CL, the small value of this term may be achieved with a larger value of the sum and a weaker phase tilt. Note that in a continuous model exactly $\bar{q}_y = 0$ is needed to have no phase tilt in the CL,

but in a discrete model \bar{q}_y has to decrease beyond a small threshold.

The change in the wave PV amplitude is explained by looking at Eq. (8): the local growth rate increases as \bar{q}_y increases and as the local wave PV amplitude decreases, relative to other points in space. This implies that if \bar{q}_y decreases at some point then the local amplitude would reduce there, relative to other points, until the change in $Q(\hat{y}, j)/Q(y, i)$ would balance the change in \bar{q}_y .

In the example shown above \bar{q}_y is reduced on the inner sides of the upper-layer CLs, and as a result the wave PV amplitude decreases near the jet flanks and the phase tilt near the CLs is reduced. The induced streamfunction loses its meridional phase tilt, consistent with a decrease in barotropic decay and an increase in growth rate.

Figure 5 shows the domain-averaged energy conversions from the mean flow to the wave [baroclinic: $\overline{U_T 2\lambda^2 (v'_M \psi'_T)}$; barotropic: $-\overline{U(v'\zeta')}$; and total], normalized by the domain-averaged wave energy [kinetic: $1/2(\overline{u'^2} + \overline{v'^2})$, plus available potential $2\lambda^2(\overline{\psi_T^2})$] to show their effect on the growth rate. It can be seen that during the increase in the growth rate, between $t = 5$ and $t = 17$, both the positive baroclinic energy conversion and the

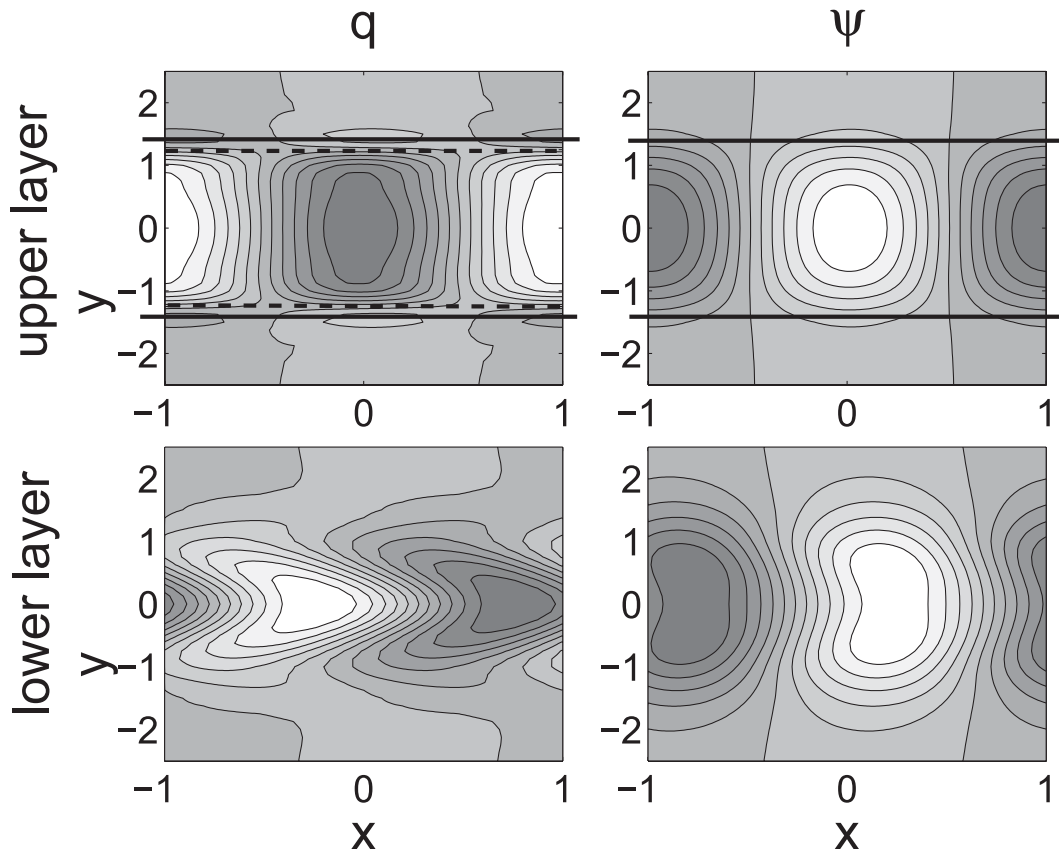


FIG. 4. As in Fig. 3, except for $t = 17$. The thick dashed lines mark the local minima of the mean PV gradient.

negative barotropic energy conversion are weakened,³ and the weakening of the latter is much stronger than the former, leading to a substantial increase in the total normalized energy conversion, during the destabilization. After $t = 17$ the energy conversion is almost entirely baroclinic. This shows that indeed the destabilization is related to a decrease in the barotropic decay, as indicated by the changes in wave structure shown above.

So far we have neglected the nonconservative terms in Eqs. (4) and (5), in our attempt to explain the change in growth rate. A direct calculation of the nonconservative contribution to the change in growth rate shows that the contribution of the radiative damping term is small relative to the PV advection term (baroclinic plus barotropic), but the contribution of the Ekman friction term is nonnegligible. We found that during the destabilization process the decay of the lower-layer wave due to Ekman friction decreases with time, which contributes to the increase in wave energy. The PV advection con-

tribution to the increase in growth rate is larger than that of Ekman friction and occurs earlier, which implies that it is more crucial for the destabilization process. We ran a simulation with no Ekman damping on the wave, while

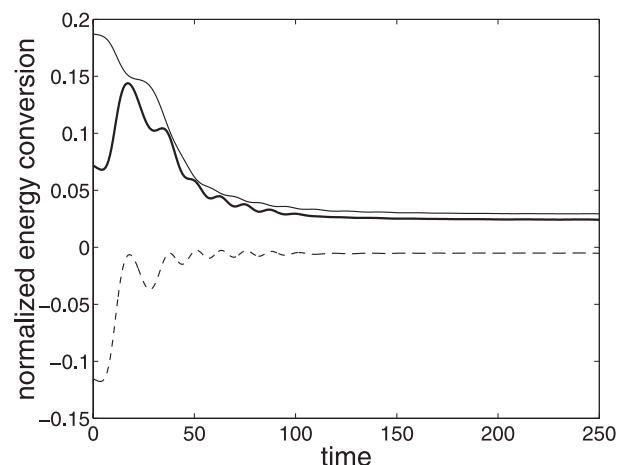


FIG. 5. Normalized energy conversions for the case $\lambda = 1.5$, $\beta = 0.5$, $\text{Ek} = 0.1$, and $\alpha = 0.05$. The thin solid line denotes baroclinic conversion; the dashed line, barotropic conversion; and the thick solid line, total conversion.

³ Note that these are normalized conversions. Both baroclinic and barotropic nonnormalized conversions, which depend on the square of the wave amplitude, actually increase with time.

all other parameters, including the Ekman friction on the mean flow, remained as in the example above. In this case destabilization still took place and a finite amplitude was reached. Lee (2009, hereafter LEE) discusses the mechanism by which the Ekman damping decreases as a result of PV mixing near the upper-layer CLs.

The phenomenon of a temporary destabilization of the mean flow by a creation of PV gradient minima near the CLs in the upper layer and a reduction in the barotropic decay was observed in all other cases which started with weak instability and ended with a large amplitude. We also checked if an increase in the vertical shear of the mean flow is responsible for the increase in the wave growth rate, and found that the vertical shear at the center of the jet temporarily increased slightly above its radiative equilibrium in some cases, but the above barotropic effect was found in all the destabilizing cases.

4. A wave amplitude transition

The phenomena of destabilization and large-amplitude equilibration, described in section 3, were found for all weakly unstable cases run with $\lambda = 1.5$ and 2 (where λ is a measure of the horizontal scale relative to the radius of deformation), and even, in some cases, in the stable part of the parameter space.⁴ Cases with larger instability of the radiative equilibrium state also produced a large-amplitude final state, but not all of them reached it after a destabilization process. For wider horizontal scales (e.g., $\lambda = 3, 4$) a large wave amplitude is not reached in all of the linearly unstable part of the parameter space. In some cases the waves equilibrate with negligible amplitude without destabilizing the mean flow. The transition between the small- and large-amplitude solutions was found to occur abruptly when model parameters (Ek , α , β) were changed gradually and also when the initial amplitude was changed. In addition, by externally forcing the PV gradient we were able to induce or inhibit this transition.

To investigate the transition as a function of the radiative damping parameter α , a series of experiments was done with $\lambda = 4$ and different values of Ek and β . For each set of these three parameters we found the value of α at which the transition occurs. Figure 6 shows

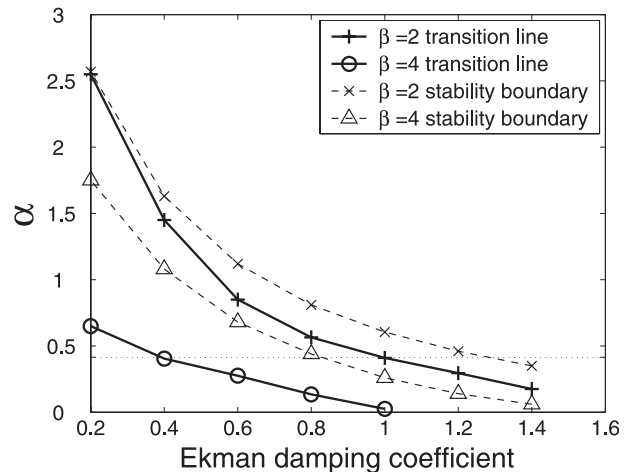


FIG. 6. The transition lines and linear stability boundaries for cases with $\lambda = 4$ and $\beta = 2$ or 4. For each β the area under the stability boundary represents cases in which the initial mean flow was linearly unstable, and the area under the transition line represents cases in which the wave reached a large amplitude. The dotted line marks the value $\alpha = 0.415$, which is referred to in the text.

the transition lines and linear stability boundaries as a function of Ek and α , for $\lambda = 4$ and $\beta = 2$ or 4. The area under the stability boundary represents the range of linear instability of the initial mean flow, and the area under the transition line represents the range in which the wave reached a large amplitude. It can be seen that the abrupt transition occurs in a wide range of the parameters. Qualitatively, we may say that the transition line follows the shape of the linear stability boundary, or that a large amplitude state is reached when the initial linear growth rate is larger. This will be explained below by a positive feedback mechanism. According to Fig. 6, the system equilibrated at small wave amplitude in a wider range of the parameter space for $\beta = 4$ compared with $\beta = 2$.⁵

As an example of a specific transition we take the case $\lambda = 4$, $\beta = 2$ and $Ek = 1$. Figure 7 shows the maximum domain averaged eddy kinetic energy reached during the model run for a few values of α , and for $\alpha = 0.45$, for a few values of the initial wave amplitude (normalized

⁴ We initialized the model with a tiny amount of the most unstable normal mode structure. In these cases, the initial growth rate was negative but very close to zero, so that even though the waves initially decayed, their effect on the mean flow near the CL was enough to decrease the barotropic decay and increase the total growth rate with time, to a point where it became positive. Thus, a large-amplitude steady state could be reached.

⁵ The structure of \bar{q}_y provides the explanation for this and for the absence of small amplitude equilibration when $\lambda = 1.5$ or 2: small-amplitude equilibration occurs when the waves stabilize the mean flow by eliminating the lower-layer negative \bar{q}_y , without causing the destabilization described in section 3. This could happen when β is large and therefore \bar{q}_y near the upper-layer CLs is large, making the described destabilization less likely. When $\lambda \sim 1$, β cannot be large in the linearly unstable part of the parameter space because the meridional curvature of \bar{U} is significant in determining the shape of \bar{q}_y ; in our jetlike configuration, this causes the lower-layer negative \bar{q}_y to be very small and vanish for large β , causing linear stability.

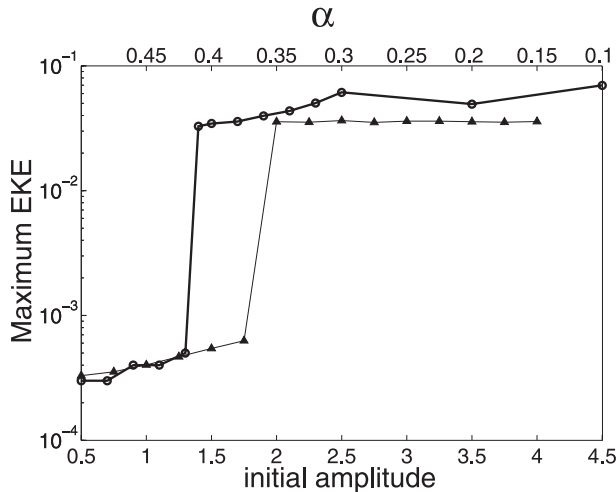


FIG. 7. Maximum domain averaged eddy kinetic energy reached during a model run for $\lambda = 4$, $\beta = 2$, and $Ek = 1$ as a function of α (thick solid line, circles), and as a function of the initial wave amplitude for $\alpha = 0.45$ (thin solid line, triangles).

by the control initial amplitude used in the previous experiments). It is seen that the eddy kinetic energy changes abruptly from the order of 10^{-4} to the order of 10^{-2} as α decreases below a certain threshold, or the initial wave amplitude increases above a certain threshold. The large amplitude waves have a domain averaged kinetic energy comparable to that of the mean flow (which is initially 8.6×10^{-2}). Note that the initial wave amplitude dependence implies the existence of multiple equilibria in the linearly unstable regime.

A destabilization of the kind shown in section 3, which was found in all other weakly unstable large amplitude cases, may explain the abrupt transition in the following way—when the wave reaches a large enough amplitude, the change it induces in the mean flow causes a destabilization, and this destabilization in turn causes a further increase in the wave amplitude, thus forming a positive feedback loop. The loop is halted when the mean flow has changed enough to decrease the baroclinic growth, or when the reduction in barotropic decay stops, because of a saturation of the CL region. Which happens earlier depends on model parameters.

The cases in which the waves did not reach a large amplitude are then cases in which the waves did not grow enough to destabilize the mean flow and initiate the positive feedback. This scenario can be confirmed by comparing cases below and above the critical threshold. Figure 8 shows the instantaneous wave growth rates as a function of time for the cases $\lambda = 4$, $\beta = 2$, $Ek = 1$ with $\alpha = 0.42$ and $\alpha = 0.41$, which are, as seen in Fig. 7, above and below the critical α for the amplitude transition, respectively. The wavenumber in both cases is $k = 3.6$. It

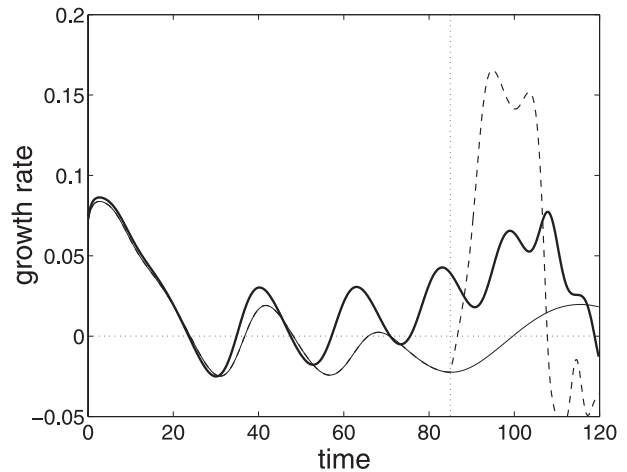


FIG. 8. Instantaneous wave growth rates as a function of time for the case $\lambda = 4$, $\beta = 2$, $Ek = 1$ with $\alpha = 0.41$ (thick solid line) and $\alpha = 0.42$ (thin solid line) and also for $\alpha = 0.42$ when \bar{q}_y is modified at $t = 85$ (thin dashed line; see text). Horizontal dotted line marks zero growth rate and vertical dotted line marks $t = 85$.

is seen that until around $t = 30$ the two growth rates evolve almost identically, after which they begin to differ increasingly with time, with the $\alpha = 0.41$ case having a large growth rate which brings its amplitude to values comparable with the mean flow, while in the $\alpha = 0.42$ case, the growth rate oscillates around zero, indicating a statistically steady state. The main difference between the normalized energy conversions of the two cases, during the destabilization stage (not shown), is in the barotropic decay—for the $\alpha = 0.42$ case it is roughly constant, while for the $\alpha = 0.41$ case it decreases in time.

The extremely different time development of the two initially similar cases, together with the two-phase dynamics that is seen in Fig. 7, raise the possibility that the system has two attractors—one which describes a state with large wave amplitude and a modified mean flow and the other having a small wave amplitude with a mean flow similar to the radiative equilibrium flow.

In section 3 we argued that the destabilization of the mean flow seen in the large amplitude cases is mainly through a reduction in the mean PV gradient on the inner sides of the upper-layer CLs. To examine this we ran the model with the same parameters as in the small amplitude case discussed above ($\lambda = 4$, $\beta = 2$, $Ek = 1$, and $\alpha = 0.42$), and at a specific time we artificially reduced the PV gradient in a tiny region (one grid point) on the inner sides of the upper-layer CLs, and forced it to remain small for the rest of the run. We specified only the PV gradient in Eqs. (4) and (5) so that the zonal mean wind field was not affected by this change. Figure 8 shows also the instantaneous growth rate as a function of time for a case where the PV gradient is reduced to a

value of 2, near the CLs, starting at $t = 85$. The forced change in the PV gradient indeed caused an increase in the growth rate and led to a large amplitude state. A closer inspection showed that the decrease in the wave PV amplitude at the jet flanks and the reduction in barotropic decay, mentioned in section 3, also occurred in this case after $t = 85$, indicating that this change triggered a transition between the two regimes. We also did the opposite experiment, where we ran a “destabilizing” case, and artificially restricted the PV gradient from decreasing below a certain value near the CLs. As expected, this inhibited the destabilization (not shown). This explicitly shows strong sensitivity to the CL region.

5. Steady-state maintenance

In order for the system to be in steady state with finite amplitude waves, the mean flow needs to be linearly neutral, when taking into account also the damping on the wave [Eqs. (4) and (5)]. In the presence of surface friction and radiative damping, this is achieved while the wave draws energy from the mean flow by baroclinic growth. The mean flow steady state requires that the wave fluxes balance the radiative forcing and surface friction [Eqs. (1)–(3)]. Since the wave, in equilibrium, draws energy from the mean flow, the nonconservative terms need to restore the energy source of the mean flow, specifically, its vertical shear.

Looking again at the case analyzed in section 3, Fig. 5 shows that at steady state the wave still extracts energy from the mean flow, and the energy conversions, which are weaker than they are at the linear growth stage, are almost totally baroclinic. This weak growth is balanced by the damping terms. The weakening of the baroclinic energy conversion is due to a decrease in the vertical phase tilt of ψ' , and an increase in the PV gradient at the lower layer, which becomes close to zero at the center.

To see how the mean vertical shear is maintained, we look at the different contributions to the growth rate of \bar{U}_T (its logarithmic time derivative) at $y = 0$ (Fig. 9). Each of the contributions, of Ekman friction, radiative damping, heat flux and momentum flux include the direct contribution [Eq. (2)] and the indirect contribution through the response of the mean meridional circulation [Eq. (3)]. At steady state ($150 < t < 250$) there is balance between the radiative damping, Ekman friction and momentum flux, which act to build the shear, and the heat flux, which acts to destroy the shear.

To check the role of radiative damping and Ekman friction in maintaining a steady state, we repeated the experiment, with the mean flow radiative damping and Ekman friction set to zero, each separately and together,

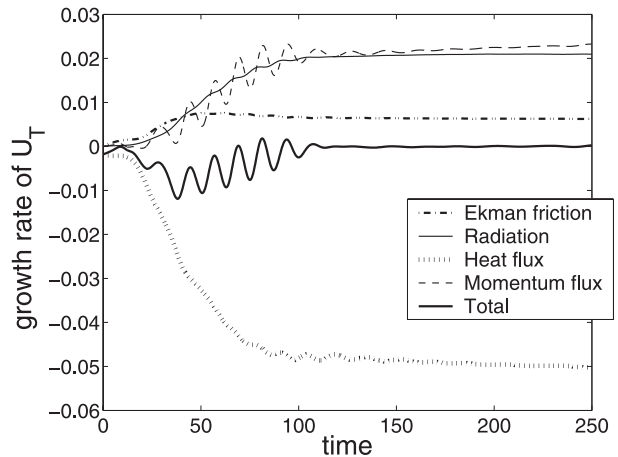


FIG. 9. The different contributions to the growth rate of \bar{U}_T at $y = 0$ as a function of time for the model parameters $\lambda = 1.5$, $\beta = 0.5$, $\text{Ek} = 0.1$, and $\alpha = 0.05$.

keeping the wave damping terms the same. Turning off radiative damping allowed the destabilization process to take place, but the system slowly decayed to a wave free neutral state after that, indicating that its presence is necessary for the steady-state vertical shear maintenance. Ekman friction on the other hand, is necessary for maintaining a steady state against the action of wave momentum fluxes, so that when it was turned off the system oscillated [Eq. (1)]. The case with no radiative damping and no Ekman friction was very similar to the case without radiative damping, except that the maximum wave amplitude reached before the decay stage was smaller. Thus Ekman friction on the mean flow contributes to the final amplitude and to the stability of the steady state.

Robinson (2006) defines a self-maintaining jet as one for which, at steady state, the baroclinic waves keep the baroclinicity of the mean flow above its radiative equilibrium value at the same latitude where they grow. He further showed that a self-maintaining jet would have a negative second derivative of the upper-layer PV flux at the point of maximum baroclinicity, where the instability is largest. Looking at the steady-state \bar{U}_T and $(v'q')_1$ in our large amplitude runs (not shown) we do not find a self-maintaining jet according to Robinson’s definition, because the vertical shear at steady state is below the radiative equilibrium value at the center and consistently, the upper-layer PV flux has a minimum point at the same place. Nevertheless, a steady state with finite amplitude waves is maintained.

A few experiments were done to check whether the destabilization process described in section 3 is necessary for reaching a large wave amplitude also in highly unstable cases. The instability was increased either by taking $\beta = 0$, by setting only the damping coefficients of

the wave to zero, keeping the mean flow damping the same, or by increasing the width of the jet.

For $\beta = 0$, with $\lambda = 1.5$, $Ek = 0.1$, and $\alpha = 0.05$, a large wave amplitude was reached, though no destabilization was observed. In this case the upper-layer PV gradient had negative values at the flanks of the jet, which enabled barotropic growth, in addition to the baroclinic growth. The growth rate decreased with time, but since it was large at the initial stage (about 0.13) a large amplitude state was reached.

For the same parameters, but with $\beta = 0.5$ and no damping on the wave, the destabilization by a reduction of the barotropic decay did occur, but was less significant, since the initial growth rate was already very large (about 0.9).

An experiment was done with the parameters of the example discussed in section 3 ($\lambda = 1.5$, $Ek = 0.1$, $\alpha = 0.05$, $\beta = 0.5$), but with a doubled jet width, and the channel boundary changed to $y_{\max} = 10$. In this case the wave reached an amplitude of 3×10^{-3} , which is between the small and large amplitude regimes (as seen in Fig. 7), before any destabilization occurred. Later, the barotropic decay decreased, the growth rate increased, and the wave reached a large final amplitude.

We conclude from these findings that the destabilization by a reduction of the barotropic decay is necessary for reaching a large wave amplitude in this model at weak instabilities, but is not always significant at high instabilities.

6. Summary and discussion

We examine in detail the dynamics leading to an abrupt wave amplitude transition in the wave–mean flow interaction system of the quasigeostrophic equations with two layers in the vertical and the β -plane assumption, when the mean flow is jetlike. The quasi-linear assumption, which neglects wave–wave interactions, is used to trace the basic wave–mean flow dynamics, which stand in the core of the fully nonlinear system.

A large wave amplitude, comparable to the mean flow, is reached after a period of time where the wave destabilizes the mean flow by reducing the PV gradient near the upper-layer CLs. Though the mean flow changes act, as expected, to reduce baroclinic growth, the accompanying reduction in the mean PV gradient near the CL causes a relatively large reduction in the barotropic decay, compared to the reduction in the growth, so that the net growth (baroclinic growth minus barotropic decay) actually increases. This destabilization persists for a while through a positive feedback loop: as the wave grows, its effect on the mean flow becomes stronger, the PV gradient is further reduced next to the CLs, the mean

flow becomes less stable and the wave grows even more. Because of this positive feedback the system is able to reach one of two very distinct final states: a state with wave amplitudes comparable to the mean flow or a state with negligible wave amplitudes. Consistent with the positive feedback mechanism described, the transition between the two cases is abrupt as one of the model parameters or initial conditions is changed.

Ekman friction and radiative damping are not crucial for the destabilization feedback to take place. Ekman friction on the wave is seen to decrease during the destabilization process (LEE), but it is apparently less important than the above barotropic effects. Nonconservative terms for the mean flow are, however, important for maintaining the vertical shear of the mean flow against destruction by the wave heat flux, thus enabling a statistically steady state with large wave amplitude to exist. The radiative damping to an equilibrium state clearly balances any tendency to divert the mean flow away from this equilibrium state and thus restores the energy taken away from the mean flow by the wave. Barnes and Young (1992) claim that the contribution of the Ekman friction to the maintenance of the wave amplitude is through its suppression of the barotropic governor. Lee and Held (1991) and Robinson (2000) attribute it to the maintenance of the vertical shear through the weakening of the surface westerlies. The results shown in this paper support the latter assumption.

As implied by previous studies, we find a major role for the reduction of PV gradients near the CL. We show that reducing the PV gradient artificially near the CL, without changing the mean wind, is enough to cause a transition from the low-amplitude regime to the large-amplitude regime. Our quasi-linear setting enables us to show explicitly how the wave structure is affected by this change in PV gradient and how this, in turn, reduces the barotropic decay. We use a PV kernel approach in our explanation (Heifetz and Methven 2005; Harnik and Heifetz 2007) rather than the wave propagation approach often used to explain CL effects, which is based on the Wentzel–Kramers–Brillouin (WKB) assumptions and is not strictly valid for baroclinic waves in the troposphere. We show, by looking at both the data of the simulations and the linear equations for the wave, that a reduction in the PV gradient near the CLs causes the upper-layer PV of the wave to be less tilted near the CLs and causes its amplitude to decrease near the jet flanks. The induced upper-layer streamfunction becomes much less meridionally tilted, and this results in less barotropic decay by inward momentum flux.

The results of this study are based on a quasi-linear model in which wave–wave interactions are ignored. These interactions are clearly important in shaping the

mean flow evolution; however, in the range of parameters studied in this paper, we do not expect them to qualitatively alter the picture obtained above because effects that are related to wave–wave dynamics are less pronounced in this parameter range. The inverse energy cascade is expected to be suppressed by friction, the β effect, and the narrowness of the baroclinic region (Pavan and Held 1996; Zurita-Gotor 2007). At large supercriticalities, waves might reach nonlinear saturation amplitudes before PV mixing at the CL will affect the dynamics; however, for the weak supercriticalities produced in this parameter range, the CL dynamics are expected to be important in the fully nonlinear model. The inclusion of wave–wave interactions is expected to create only a quantitative difference, since it would make the mixing of the mean PV by the waves more efficient (Haynes and McIntyre 1987). Support for this is found in Lee and Held (1991), who found similar dynamics in the quasi-linear and nonlinear versions of this two-layer model. O’Gorman and Schneider (2007) show that a GCM without wave–wave interactions is able to capture many of the features of the full GCM, including the shape of the energy spectrum and the dominant wavenumber.

Another approach to modeling the equilibrated state is to view the role of nonlinearities primarily as stochastic noise on a marginally stable state, which continuously excites the waves and keeps them at a finite-amplitude state (DelSole 2004). The quasi-linear part of the dynamics is present in these models; thus, we expect the same dynamical interactions to play a role. In particular, CL dynamics may play an important role in allowing the waves to reach a finite amplitude, even in the linearly stable regime. Moreover, stochastic models also exhibit regime transitions (e.g., Farrell and Ioannou 2003). It is possible that a similar positive feedback between wave amplitude and the contribution of barotropic decay to the perturbation growth gives rise to the observed transitions in these models. We note, however, that stochastic models include all zonal wavenumbers whereas ours includes only one, but we do see a tendency for specific wavenumbers to arise both in models and in observations, so the existence of more than one wavenumber may not alter the picture too much.

Finally, the sphericity of the earth, which was neglected in this model, affects the wave–mean flow interaction in several ways. The spherical geometry results in the disappearance of the CL from the poleward flank of the jet for many wavenumbers. In addition, the latitudinal variation of f and β affects not only the mean flow (e.g., the meridional PV gradients) but also the internal wave dynamics (e.g., through the stretching term). Nonetheless, we do find evidence in spherical models for a sensitivity of wave evolution to the CL region (Thorncroft et al. 1993;

Robinson 2006) as well as to thermal and Ekman damping (Barnes and Young 1992), but other processes, such as a change in wave phase speed (e.g., Robinson 2006), can come into play. How the quasi-linear dynamics described above are manifest under these settings thus requires further investigation and will be the subject of future investigations.

Acknowledgments. The authors wish to thank two anonymous reviewers for their insightful comments, and Eyal Heifetz and Sukeyoung Lee for illuminating discussions. This work was funded by a European Union Marie Curie International Reintegration Grant (MIRG-CT-2005-016835) and Israeli Science Foundation Grants 1370/08 and 1084/06.

APPENDIX

The Numerical Model

We solve the two-layer β -plane quasigeostrophic equations for the perturbations from a zonal mean [Eqs. (4)–(5)] and for the zonal mean flow [Eqs. (1)–(3)]. The perturbation equations include only first-order terms, whereas the mean flow equations include second-order perturbation terms. We use the conventional Eulerian mean equations (Holton 1992, section 10.2.1) and the perturbation is assumed to consist of a single zonal wavenumber (k). The two layers are located between two rigid boundaries, representing the surface and the tropopause, similar to Phillips’ model (Phillips 1951). Radiative damping to an equilibrium state and Ekman surface friction are included.

Equations (1)–(5) are nondimensionalized as stated in Table A1 and are written in terms of the barotropic and baroclinic components (subscripts M and T , respectively).

The winds are assumed to be geostrophic: $(u'_j, v'_j) = (-\partial\psi'_j/\partial y, \partial\psi'_j/\partial x)$, $\zeta'_j = -k^2\psi'_j + \partial^2\psi'_j/\partial y^2$, where $j = 1$ and 2 refer to the upper and lower layers, respectively. The barotropic and baroclinic perturbation PV thus become $q'_M = \zeta'_M$, and $q'_T = \zeta'_T - 2\lambda^2\psi'_T$, whereas the barotropic and baroclinic mean PV gradients become $(\partial\bar{q}/\partial y)_M = \beta - \bar{U}_{M,y}$ and $(\partial\bar{q}/\partial y)_T = -\bar{U}_{T,y} + 2\lambda^2\bar{U}_T$.

TABLE A1. Nondimensional variables.

Meridional coordinate	$y = y^*/L$
Zonal wavenumber	$k = k^*L$
Time coordinate	$t = t^*U_0/L$
Geostrophic streamfunction	$\psi = \psi^*/LU_0$
Ageostrophic meridional wind	$\bar{v}'_a = \bar{v}'^*_a Lf/U_0^2$

* Here L is a typical horizontal length scale, U_0 is a typical velocity scale for the zonal mean wind, and f is the Coriolis parameter. The dimensional variables are denoted by an asterisk.

TABLE A2. Model parameters. Here N is the Brunt–Väisälä frequency, ΔZ the vertical length scale, Bu the Burger number, τ_{Ekman} a typical time scale for Ekman surface friction, τ_{Rad} a typical time scale for radiative damping, and β^* the dimensional Coriolis parameter gradient.

Parameter	Expression	Description
λ	$1/\sqrt{Bu} \equiv fL/N\Delta Z$	Ratio between the horizontal length scale and Rossby radius of deformation
Ek	$L/U_0\tau_{\text{Ekman}}$	Ratio between the advective time scale and the Ekman friction time scale
α	$L/U_0\tau_{\text{Rad}}$	Ratio between the advective time scale and the radiative damping time scale
β	β^*L^2/U_0	Nondimensional Coriolis parameter gradient

The nondimensionalization yields four nondimensional parameters λ , Ek , α , and β , which appear in Table A2.

The meridional boundaries are at $y = \pm y_{\text{max}} = \pm 5$, which is far enough from the baroclinically active zone to not affect the dynamics. The boundary condition for the mean flow is $\partial\bar{U}/\partial y = 0$ to ensure no mean PV gradients near the boundaries. Because the radiative equilibrium and initial \bar{U} are zero near the boundaries at both layers, \bar{U} remains effectively zero there throughout the integration. The boundary condition for the perturbation is $v' = \psi' = 0$. We start the integration from radiative equilibrium with no mean flow at the surface and initialize it with the most unstable normal mode perturbation.

In the meridional direction we used simple central differencing, with a grid that contains 81 points. This resolution is enough to capture the basic behavior of the system and to prevent unphysical influence of the boundaries. A few experiments were done with higher resolution and showed similar behavior. For the time integration we used the third-order Adams–Bashforth scheme.

Numerical fourth-order diffusion on the meridional direction was added to suppress the small-scale noise and physically represent the energy transfer to the unresolved scales. The diffusion coefficient was chosen by trial and error to be 0.05, large enough to remove strong grid-scale meridional gradients and small enough not to affect the large-scale features.

REFERENCES

- Barnes, J. R., and R. E. Young, 1992: Nonlinear baroclinic instability on the sphere: Multiple life cycles with surface drag and thermal damping. *J. Atmos. Sci.*, **49**, 861–878.
- DelSole, T., 2004: Stochastic models of quasigeostrophic turbulence. *Surv. Geophys.*, **25**, 107–149.
- Esler, J. G., and P. H. Haynes, 1999: Mechanisms for wave packet formation and maintenance in a quasigeostrophic two-layer model. *J. Atmos. Sci.*, **56**, 2457–2490.
- Farrell, B. F., and P. J. Ioannou, 2003: Structural stability of turbulent jets. *J. Atmos. Sci.*, **60**, 2101–2118.
- Feldstein, S. B., and I. M. Held, 1989: Barotropic decay of baroclinic waves in a two-layer beta-plane model. *J. Atmos. Sci.*, **46**, 3416–3430.
- Harnik, N., and E. Heifetz, 2007: Relating overreflection and wave geometry to the counterpropagating Rossby wave perspective: Toward a deeper mechanistic understanding of shear instability. *J. Atmos. Sci.*, **64**, 2238–2261.
- Hartmann, D. L., and P. Zuercher, 1998: Response of baroclinic life cycles to barotropic shear. *J. Atmos. Sci.*, **55**, 297–313.
- Haynes, P. H., and M. E. McIntyre, 1987: On the representation of Rossby wave critical layers and wave breaking in zonally truncated models. *J. Atmos. Sci.*, **44**, 2359–2382.
- Heifetz, E., and J. Methven, 2005: Relating optimal growth to counterpropagating Rossby waves in shear instability. *Phys. Fluids*, **17**, 064 107, doi:10.1063/1.1937064.
- Held, I. M., and V. D. Larichev, 1996: A scaling theory for horizontally homogeneous, baroclinically unstable flow on a beta plane. *J. Atmos. Sci.*, **53**, 946–952.
- Holton, J. R., 1992: *An Introduction to Dynamic Meteorology*. 3rd ed. Academic Press, 511 pp.
- Killworth, P. D., and M. E. McIntyre, 1985: Do Rossby-wave critical layers absorb, reflect, or over-reflect? *J. Fluid Mech.*, **161**, 449–492.
- Lee, S., 2009: Finite-amplitude equilibration of baroclinic waves on a jet. *J. Atmos. Sci.*, in press.
- , and I. M. Held, 1991: Subcritical instability and hysteresis in a two-layer model. *J. Atmos. Sci.*, **48**, 1071–1077.
- O’Gorman, P. A., and T. Schneider, 2007: Recovery of atmospheric flow statistics in a general circulation model without nonlinear eddy–eddy interactions. *Geophys. Res. Lett.*, **34**, L22801, doi:10.1029/2007GL031779.
- Pavan, V., and I. M. Held, 1996: The diffusive approximation for eddy fluxes in baroclinically unstable jets. *J. Atmos. Sci.*, **53**, 1262–1272.
- Phillips, N. A., 1951: A simple three-dimensional model for the study of large-scale extratropical flow patterns. *J. Meteor.*, **8**, 381–394.
- Robinson, W. A., 2000: A baroclinic mechanism for the eddy feedback on the zonal index. *J. Atmos. Sci.*, **57**, 415–422.
- , 2006: On the self-maintenance of midlatitude jets. *J. Atmos. Sci.*, **63**, 2109–2122.
- Schneider, T., and C. C. Walker, 2006: Self-organization of atmospheric macroturbulence into critical states of weak nonlinear eddy–eddy interactions. *J. Atmos. Sci.*, **63**, 1569–1586.
- Son, S. W., and S. Lee, 2005: The response of westerly jets to thermal driving in a primitive equation model. *J. Atmos. Sci.*, **62**, 3741–3757.
- Stone, P. H., 1978: Baroclinic adjustment. *J. Atmos. Sci.*, **35**, 561–571.
- Swanson, K., 2008: Coexisting turbulent climate attractors in a two-layer quasigeostrophic model. *J. Atmos. Sci.*, **65**, 2994–3001.
- Thorncroft, C. D., B. J. Hoskins, and M. E. McIntyre, 1993: Two paradigms of baroclinic-wave life-cycle behaviour. *Quart. J. Roy. Meteor. Soc.*, **119**, 17–55.
- Warn, T., and H. Warn, 1978: The evolution of a nonlinear critical level. *Stud. Appl. Math.*, **59**, 37–71.
- Zurita-Gotor, P., 2007: The relation between baroclinic adjustment and turbulent diffusion in the two-layer model. *J. Atmos. Sci.*, **64**, 1284–1300.